



Universiteit
Leiden
The Netherlands

13C MAS NMR and photo-CIDNP reveal a pronounced assymetry in the electron ground state of the special pair of Rhodobacter spearoides reaction centers

Schulten, E.A.M.; Matysik, J.; Alia, A.; Kiihne, S.R.; Raap, J.; Lugtenburg, J.; ... ; Groot, H.J.M. de

Citation

Schulten, E. A. M., Matysik, J., Alia, A., Kiihne, S. R., Raap, J., Lugtenburg, J., ... Groot, H. J. M. de. (2002). 13C MAS NMR and photo-CIDNP reveal a pronounced assymetry in the electron ground state of the special pair of Rhodobacter spearoides reaction centers. *Biochemistry*, 41(27), 8708-8717. doi:10.1021/bi025608u

Version: Publisher's Version

License: [Licensed under Article 25fa Copyright Act/Law \(Amendment Taverne\)](#)

Downloaded from: <https://hdl.handle.net/1887/3239459>

Note: To cite this publication please use the final published version (if applicable).

^{13}C MAS NMR and Photo-CIDNP Reveal a Pronounced Asymmetry in the Electronic Ground State of the Special Pair of *Rhodobacter sphaeroides* Reaction Centers[†]

Els A. M. Schulten,[‡] Jörg Matysik,^{*,‡} Alia,[‡] Suzanne Kiihne,[‡] Jan Raap,[‡] Johan Lugtenburg,[‡] Peter Gast,[§] Arnold J. Hoff,^{§,||} and Huub J. M. de Groot[‡]

Leiden Institute of Chemistry, Gorlaeus Laboratoria, P.O. Box 9502, 2300 RA Leiden, The Netherlands, and
Department of Biophysics, Huygens Laboratorium, P.O. Box 9504, 2300 RA Leiden, The Netherlands

Received January 30, 2002; Revised Manuscript Received April 26, 2002

ABSTRACT: Reaction centers of wild-type *Rhodobacter sphaeroides* were selectively ^{13}C -isotope labeled in bacteriochlorophyll and bacteriopheophytin. ^{13}C solid-state CP/MAS NMR and photo-CIDNP were used to provide insight into the electronic structure of the primary electron donor and acceptor on the atomic scale. The first 2-dimensional photochemically induced dynamic nuclear polarization (photo-CIDNP) ^{13}C – ^{13}C solid-state MAS NMR spectra reveal that negative charging of the two BChl rings of the primary donor is involved in ground-state tuning of the oxidation potential of these cofactors in the protein via local electrostatic interactions. In particular, the ^{13}C shifts show moderate differences in the electronic structure between the two BChl molecules of the special pair in the electronic ground state, which can be attributed to hydrogen bonding of one of the BChl molecules. The major fraction of the electron spin density is strongly delocalized over the two BChl molecules of the special pair and the photochemically active BPhe. A small fraction of the π -spin density is distributed over a fourth component, which is assigned to the accessory BChl. Comparison of the photo-CIDNP data with “dark” NMR spectra obtained in ultra high field indicates a rigid special pair environment upon photoreaction and suggests that structural changes of the aromatic macrocycles of the two BChl molecules of the special pair do not significantly contribute to the reorganization energy associated with the charge-transfer process.

Photosynthesis is the process that uses solar energy for the synthesis of organic compounds. The initial process of light-induced electron transfer occurs in photosynthetic reaction centers (RCs). The structures of the RC of several purple bacteria were resolved by X-ray diffraction (1–4). They resemble the photosystem II (PS–II) water splitting enzyme from plants (5). The bacterial *Rhodobacter* (*Rb.*) *sphaeroides* protein complex consists of 3 polypeptides, H,

[†] This research was supported by grants from the Council for Chemical Sciences of The Netherlands Organization for Scientific Research (CW-NWO) to J.L. (700-37-005) and H.J.M.d.G. (PIONIER). J.M. acknowledges a Casimir-Ziegler award of the Academies of Sciences in Amsterdam and Düsseldorf. The Ultra High Field spectrometer was financed in part by an EU demonstration project (Bio4-CT97-2101).

* To whom correspondence should be addressed. E-mail: ssnmr@chem.leidenuniv.nl. Fax: +31-71-5274603. Telephone: +31-71-5274539.

[‡] Leiden Institute of Chemistry.

[§] Department of Biophysics.

^{||} Deceased on April 22, 2002.

¹ Abbreviations: 1-D, one-dimensional; 2-D, two-dimensional; σ , chemical shift; ALA, δ -aminolevulinic acid; B, accessory bacteriochlorophyll; BChl, bacteriochlorophyll; BPhe, bacteriopheophytin; C, carotenoid; Chl, chlorophyll; CP, cross polarization; CRAMPs, combined rotation and multiple pulses; His, Histidine; I, primary electron acceptor; MAS, magic-angle spinning; Mg, magnesium; NMR, nuclear magnetic resonance; P, primary electron donor (“special pair”); PBG, porphobilinogen; Phe, pheophytin; photo-CIDNP, photochemically induced dynamic nuclear spin polarization; PS–II, photosystem II; Q, ubiquinone; *Rb.*, *Rhodobacter*; RC, photosynthetic reaction center; RFDR, radio-frequency-driven recoupling; TOSS, total sideband suppression; TPPM, two-pulse–phase modulation; WT, wild-type.

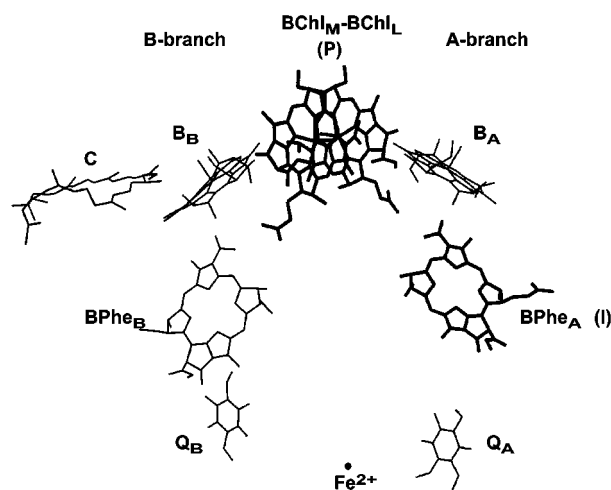


FIGURE 1: Arrangement of cofactors in RC of *Rhodobacter sphaeroides* WT. The aliphatic chains of BChl, BPhe, and Q have been omitted for clarity. The cofactors that participate in the photo-CIDNP experiment (P and I) are depicted in bold.

L, and M, and nine cofactors that are arranged in two nearly symmetric branches. The electron transfer reaction proceeds almost exclusively via the “active” A-branch, while the B-branch is “inactive” (Figure 1). Four bacteriochlorophylls (BChl) are coordinated to the L and M polypeptides. Two of the BChl form the dimer BChl_L–BChl_M, often named the “special pair” (P). The remaining two accessory BChls, B_A and B_B, are monomers. In addition, the protein contains two

bacteriopheophytins (BPhe_A and BPhe_B), two ubiquinones-10 (Q_A and Q_B), and a non-heme iron (Fe²⁺). In the RC of wild-type (WT) *Rb. sphaeroides*, a carotenoid (C) is present. This tenth cofactor breaks the overall symmetry of the cofactor arrangement and is located near B_B (4).

After photochemical excitation, an electron is emitted from the primary electron donor P and transferred to the primary electron acceptor BPhe_A (I) within 3 ps (6), forming the radical pair state P^{•+}I^{•-}. Although the structure of the protein complex and the kinetics of electron transfer after photoexcitation are characterized in detail for several RC species, it is not exactly clear if and how the electronic structure of the BChl molecules of P is tuned in the ground state to facilitate the emission of an electron in the electronically excited state. In addition, it is thought that electron transfer involves structural reorganization (7). However, it is not known if and how the BChl and BPhe ring systems contribute to the reorganization energy by structural changes.

The two BChl molecules of P overlap in ring I with an intermolecular distance of approximately 3.5 Å. The Mg atoms of both BChls are coordinated by a histidine ligand (His M202 and His L173). Each BChl has four possible sites for hydrogen bonding, i.e., 3-acetyl, 13¹-keto, 13³-methoxy and 17³-carboxy (Figure 2), of which the 3-acetyl and 13¹-keto groups are part of the conjugated π -system. It was established that an addition of hydrogen bonds correlates with an increase in midpoint oxidation potential (8). Structural and spectroscopic data have provided convincing evidence that the 3-acetyl group of P-BChl_L forms a hydrogen bond with His L168 (9, 10).

The electronic structures of P^{•+} and P* have been thoroughly investigated at different time scales with various spectroscopic techniques. Both intermediates of the photochemical cycle of the RC are asymmetric (11, 12). It was proposed that the excited state P* is electronically asymmetric and that this electronic asymmetry is related to the hydrogen bonding environment of the keto groups (12). In contrast, knowledge of the precise electronic structure of P in the ground state is limited. X-ray crystallography does not provide sufficient resolution. Solid-state NMR spectroscopy is a powerful method to probe the electronic ground state of membrane proteins (13, 14). For instance, recently obtained ¹⁵N solid-state NMR data from [¹⁵N-His] enriched bacterial RCs indicate that the BChl-histidine complexes of P are negatively charged (15). Photochemically induced dynamic nuclear polarization (photo-CIDNP) provides another possibility to investigate the electronic structure of the primary donor (P) and acceptor (I) of RCs with solid-state MAS NMR (16). The interaction of nuclei with the photochemically produced electron pair enhances the net nuclear polarization by more than 2 orders of magnitude. The photo-CIDNP chemical shift information refers to the electronic structure of the diamagnetic ground state after the photo-reaction and recombination. Photo-CIDNP provides a unique chance to probe the electronic structure of the photochemically active regions of RCs in the ground state on the atomic scale, while the photo-CIDNP intensity is related to the electron spin density distribution in P^{•+}I^{•-}. The details of the mechanism are currently under discussion (17–19). Recent experiments demonstrated that the initial nuclear polarization pattern is modified by internuclear spin diffusion (20, 21).

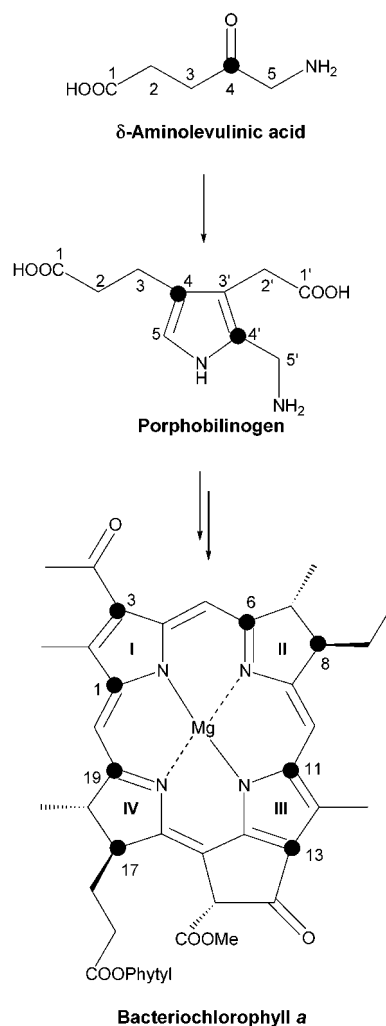


FIGURE 2: Schematic representation of the biosynthesis of BChl *a* starting from δ -aminolevulinic acid (ALA). The positions of the ¹³C-labels are indicated with filled circles (●). BPhe *a* is a derivative of BChl *a*, in which the magnesium is replaced by two hydrogen atoms. The numbering of BChl *a* is according to the IUPAC nomenclature.

In the present study, the preparation and solid-state NMR characterization of RCs with site-directed ¹³C enriched BChl and BPhe obtained from cultures of *Rb. sphaeroides* WT grown in the presence of 99% [4-¹³C]-ALA are reported. ALA is a biosynthetic precursor of BChl and BPhe, and the extent of incorporation was determined by mass spectrometry. To probe the ground-state electronic structures of P at the atomic scale before and after a photochemical cycle, the labeled preparations were first measured with 2-D ultra-high-field cross polarization magic-angle spinning (CP/MAS) solid-state dipolar correlation spectroscopy without illumination followed by ¹³C photo-CIDNP MAS NMR. Three BChl species with similar chemical shifts and one BChl with different chemical shifts can be resolved, while the two BPhe cofactors appear similar to each other. The combination of partial ¹³C enrichment and photo-CIDNP yields a strong enhancement of the NMR intensity and reduces the number of signals. The two-dimensional ¹³C-¹³C photo-CIDNP solid-state MAS NMR experiments presented here allow the chemical shift assignments for the labeled carbons that participate in the photo-CIDNP process. Three cofactors are identified as the two BChls from P and the primary electron

acceptor BPhe_A (I), and a fourth weaker signal component appears to originate from monomeric BChl. The chemical shifts of responses from corresponding carbon nuclei from the two BChl within P are different. This shows that the electronic structure of P is asymmetric in the ground state. The shifts detected for the “dark” CP/MAS NMR data set and the results from the photo-CIDNP are the same within the resolution of the NMR experiments and provide strong evidence that both the electronic structure and the spatial structure for the rings of the two BChls of P and the photochemically active BPhe are essentially conserved during the photochemistry and its associated reorganization process.

MATERIALS AND METHODS

Preparation of ¹³C-Labeled RCs. δ-Aminolevulinic acid (ALA) is the initial unique biosynthetic precursor for naturally occurring tetrapyrroles, including BChl and BPhe (22). ¹³C-ALA incorporated into BChl has been used as a tracer for the elucidation of its biosynthetic pathway (23, 24). Two molecules of ALA are asymmetrically condensed to form the pyrrole porphobilinogen (Figure 2). Four molecules of PBG tetramerize, and prior to macrocycle ring closure, the last pyrrole ring (ring IV) is inverted via a spiro-intermediate. This explains why BChl and BPhe are asymmetric in their macrocycle backbones. Starting from ALA ¹³C enriched at a single position, PBG will be doubly enriched, and the resulting BChl and BPhe will be 8-fold labeled. When [4-¹³C]-ALA is fully incorporated, the four pyrrole rings will be pairwise labeled, according to pair I (C-1/C-3), pair II (C-6/C-8), pair III (C-11/C-13), and pair IV (C-17/C-19). Pair I and pair IV are separated by a single unlabeled carbon, while pairs I and II and pair II and III are separated by two unlabeled carbons. Finally, pair III and IV are separated by three unlabeled carbons (Figure 2).

Cultures of *Rb. sphaeroides* WT (480 mL) were grown anaerobically in the presence of 1.0 mM [4-¹³C]-δ-aminolevulinic acid·HCl (COOHCH₂CH₂13COCH₂NH₂·HCl), which was purchased from Cambridge Isotope Laboratories (99% ¹³C-enriched). The cultures were allowed to grow for 7 days in light. Prior to harvesting the cells for the preparation of the RCs, a 4 mL aliquot was taken from the culture to determine the extent of incorporation from the [4-¹³C]-ALA in the medium. The culture was centrifuged for 10 min at 5500 × g, and the combined pellet was resuspended in 40 mL 0.1 M phosphate buffer (pH = 7.5). The RCs were isolated as described by Shochat et al. (25). A protein/pigment ratio A₂₈₀/A₈₀₂ = 1.2 was measured in the absorption spectrum to assess the purity of the samples. Approximately 15 mg of the labeled RC protein was used for the NMR experiments.

Determination of the ¹³C Incorporation. The ¹³C incorporation of [4-¹³C]-ALA that was added to the growth medium was determined from BChl, which is abundantly present in the organism. BPhe is formed from BChl after loss of Mg during incorporation of the pigment into the protein (26). It is therefore assumed that the extent of incorporation in BPhe and BChl is identical. The 4 mL sample was centrifuged for 30 min at 5000 × g, and the supernatant was removed. The cell pellet was resuspended in acetone/methanol (7/2 v/v) and shaken. After standing for approximately 20 min, the cells were centrifuged for 30 min (5000 × g), and the supernatant was transferred into a flask.

The procedure was repeated until the cell pellet was gray/white. The solvents were evaporated in vacuo, and the pigments were dissolved in 5 mL acetone. One hundred microliters of this solution was diluted with acetone/MeOH/H₂O (7/2/1 v/v) to 1 mL, and the optical absorption spectrum was recorded. A concentration of 4 μM for the BChl was calculated from the optical absorption at 773 nm using an extinction coefficient ε = 75 mM⁻¹cm⁻¹ (27). The crude pigment extract was loaded on a cellulose-20 column with light petroleum ether (40/60), and the column was washed with petroleum ether (24). Carotenoids and BPhe were first eluted with petroleum ether/acetone (33/1 v/v), and finally BChl was eluted with petroleum ether/acetone (20/1 v/v). The solvent was evaporated in vacuo, and the pure BChl was stored at -20 °C in a dry nitrogen atmosphere.

The isotope constitution of the labeled BChl was analyzed with a Finnigan MAT-900 double-focus mass spectrometer (Finnigan MAT, San Jose, CA). A small fraction of the purified pigment was dissolved in water/methanol (20/80 v/v) containing 1% of acetic acid. Since the macrocycle backbone of BChl and BPhe is synthesized from eight molecules of ALA, a maximum of eight ¹³C labels can be incorporated in BChl or BPhe. The isotopic pattern was investigated around *m/z* = 911 ([M]⁺; C₅₅H₇₄MgN₄O₆). For every experiment, at least seven scans spanning a region from *m/z* = 850–950 were accumulated. An unlabeled control was grown under similar conditions as those for the labeled samples. The isotopic pattern of this reference was recorded prior to the measurement of the labeled sample. The ratios of the peak intensities were calculated for the reference spectrum. The label incorporation was obtained via an iterative procedure, which is described in detail in ref 28. Via this method, the fractions *P_n* of the eight different labeled BChls and natural abundance BChl can be determined. The total incorporation *P_{tot}* was calculated by the weighted sum:

$$P_{\text{tot}} = \sum_{n=0}^8 \frac{n}{8} \times P_n \quad (1)$$

where *n* stands for the number of labels present in an isotopomer and *P₀* is the corresponding fraction of unlabeled BChl estimated from the isotopic labeling pattern detected with the mass spectrometer.

MAS NMR Measurements. ¹³C NMR data were collected from the labeled BChl *a* in acetone-*d*₆ with a DMX-600 spectrometer (Bruker, Karlsruhe, Germany), and the ¹³C shifts are referenced to the shifts of natural abundance ¹³C carbonyl response for the acetone-*d*₆ with σ = 206 ppm.

Cross-polarization solid-state MAS data for samples in the “dark” were collected in ultra high field with a DSX-750 NMR spectrometer (Bruker, Karlsruhe, Germany) equipped with a double-resonance MAS probe operating at 750 MHz for ¹H and 188 MHz for ¹³C. The experiments were performed at a temperature *T* = 223 K and using a spinning frequency of ω_r/2π = 12 kHz. A 4 mm rotor with a CRAMPs insert was loaded with 2 mg labeled RCs and was frozen slowly with liquid-nitrogen-cooled bearing gas, using slow spinning with 600 Hz. For the 1-D CP/MAS NMR spectrum, 12k scans were recorded in 2k data points with a sweep width of 60 kHz. Zerofilling to 4k and an exponential line broadening of 100 Hz were applied prior to Fourier

transformation. 2-D homonuclear (^{13}C – ^{13}C) dipolar correlation spectra were recorded with the RFDR technique (29–31) using mixing times of 2.3 and 4.6 ms. In the t_2 dimension, 2k data points with a sweep with of 94 kHz were recorded. Zerofilling to 4K and an exponential line broadening of 100 Hz was applied prior to Fourier transformation. In the t_1 dimension, 180 scans using 1k data points were recorded, and a linear prediction was performed using 66 points (32). A sine-squared apodization shifted by $\pi/2$ was used prior to Fourier transformation.

Photo-CIDNP MAS NMR experiments were performed with a DMX-400 NMR spectrometer (Bruker, Karlsruhe, Germany) that was equipped with a double-resonance MAS probe operating at 396.5 MHz for ^1H and 99.7 MHz for ^{13}C . The illumination setup has been described in detail elsewhere (33). A sample containing 10 mg of the RC complex was loaded into a clear sapphire 4 mm rotor, and ^{13}C MAS NMR spectra were recorded at a temperature of 220 K with $\omega_r/2\pi = 4$ kHz or $\omega_r/2\pi = 5$ kHz. Several minutes before the experiment was started, 4 μL of 10 mM ascorbic acid was added, and the acceptor site Q_A was photoreduced in situ. The sample was continuously illuminated during the course of the experiment. Photo-CIDNP spectra were collected with a Hahn echo-pulse sequence and two pulse-phase modulation (TPPM) proton decoupling (34). A recycle delay of 12 s was used. To distinguish absorptive and emissive signals, we recorded a spectrum of solid [U - ^{13}C]-tyrosine $\cdot\text{HCl}$ prior to the experiment. The phase correction for this reference was essentially conserved in phasing the photo-CIDNP spectra. The 1-D “light” spectra were recorded in 2k data points with a sweep width of 50 kHz and an exponential line broadening of 25 Hz was used. Total sideband suppression (TOSS) was performed with a train of rotor synchronized Hahn echoes depleting the sideband intensities (35). For the 2-D homonuclear (^{13}C – ^{13}C) dipolar correlation spectra, an adapted RFDR pulse sequence was applied with the initial cross polarization step replaced by a $\pi/2$ pulse. The details of this adapted RFDR will be described separately in a technical note. The RDRF experiments were recorded with mixing times of 3 and 6 ms. In the t_2 dimension, 2k data points with a sweep with of 50 kHz were recorded. Zerofilling to 4k and an exponential line broadening of 25 Hz were applied prior to Fourier transformation. In the t_1 dimension, 143 scans using 1k data points were recorded, and a linear prediction was performed using 50 points (32). A sine-squared apodization shifted by $\pi/2$ was used prior to Fourier transformation.

Both the CP and photo-CIDNP MAS NMR spectra were referenced to the $^{13}\text{COOH}$ response of solid tyrosine $\cdot\text{HCl}$ at 172.1 ppm.

RESULTS

Label Incorporation. Initially, the addition of [4 - ^{13}C]-ALA to the medium for growing the *Rb. sphaeroides* WT resulted in a decrease of $\sim 25\%$ in the amount of BChl formed compared to a control experiment without the labeled ALA. After an adaptation phase where the broth was twice subcultured, the difference had vanished. In similar experiments with *Rb. sphaeroides* R26, growth was completely blocked. The inhibitory effects can be attributed to the regulatory role of ALA synthase (36). In the natural biosynthesis of BChls in *Rb. sphaeroides*, accumulation of porphyrin intermediates is prevented by an inhibition of ALA

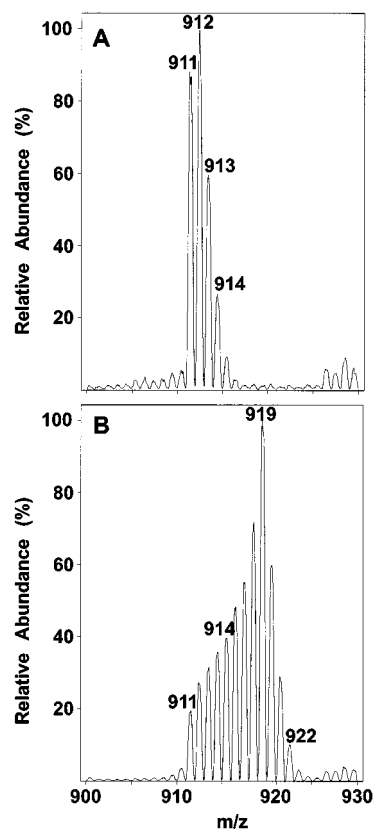


FIGURE 3: Isotopic patterns around $m/z = 911$ from natural abundance BChl (A) and $^{13}\text{C}_{0-8}$ BChl (B).

synthase in a feedback mechanism. The addition of an excess of ^{13}C -ALA to the medium bypasses the regulation of ALA synthase, which leads to the accumulation of porphyrin intermediates (37). These intermediates can be excited by light, which leads to toxic triplet porphyrin states. In *Rb. sphaeroides* R26, these excited porphyrin intermediates were lethal, while *Rb. sphaeroides* WT was still capable of growth under light growing conditions. *Rb. sphaeroides* WT contains carotenoids, while *Rb. sphaeroides* R26 is a carotenoid-deficient mutant. Possibly, the ability of *Rb. sphaeroides* WT to adapt to the relatively high concentration of 1.0 mM ALA relates to the presence of carotenoids that quench triplet states (38).

With ^{13}C NMR of the labeled BChl in solution, it was confirmed that carbons C-1, C-3, C-6, C-8, C-11, C-13, C-17, and C-19 were partially ^{13}C enriched (data not shown). These positions are indicated in Figure 2 with filled circles. Each pyrrole ring contains two ^{13}C -enriched positions separated by an unlabeled carbon. The label incorporation was determined by the analysis of the isotopic pattern of natural abundance BChl and the labeled sample (Figure 3). Due to the incorporation of unlabeled ALA produced by the de novo biosynthesis in the organism, a mixture of isotopomers with up to $n = 8$ atoms that are ^{13}C -enriched is obtained. The analysis of the isotopic pattern of the labeled sample (Figure 4B) reveals that $P_8 \approx 25\%$. The various other fractions of isotopomers (P_1 – P_7) and unlabeled BChl (P_0) are estimated between 5% and 10%. The weighted sum of these separate contributions according to eq 1 corresponds with a total incorporation $P_{\text{tot}} = 60 \pm 5\%$.

Assignment of the MAS NMR Responses. In Figure 4, the 1-D ^{13}C spectra collected from the labeled RCs with photo-

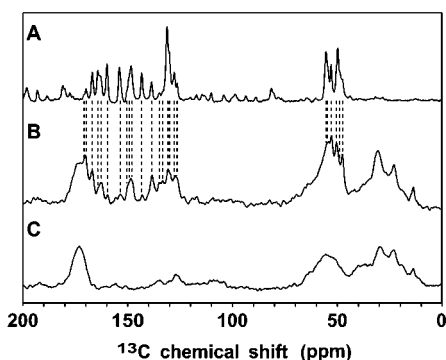


FIGURE 4: 1-D solid-state NMR spectra of the bacterial RC of *Rb. sphaeroides* WT. The 100 MHz ^{13}C photo-CIDNP MAS solid-state NMR spectrum of [$^{13}\text{C}_{0-8}$ -BChl/BPhe] RCs at 220 K at a spinning frequency of 5 kHz was obtained in 20 min (A). The “dark” spectra were recorded with ultra-high-field solid-state ^{13}C CP/MAS NMR. Data sets of [$^{13}\text{C}_{0-8}$ -BChl/BPhe]-RCs (B) and natural abundance RCs (C) were recorded at 223 K with a spinning frequency of 12 kHz. In both “light” and “dark” spectra, the labeled carbons resonate with comparable chemical shifts, which is visualized by the dashed lines.

CIDNP (A) and in the “dark” with CP/MAS (B) are shown. The data are compared with the 1-D CP/MAS spectrum collected in the “dark” from an unlabeled RC preparation (C). In both “dark” CP/MAS spectra, there is a broad natural abundance ^{13}C response between 10 and 60 ppm from the saturated carbons in the apoprotein and from aliphatic ^{13}C in the detergent. A weaker response is observed between 100 and 140 ppm from the aromatic residues, and finally a signal at 175 ppm is due to the carbonyl groups in the protein. In the “dark” CP/MAS spectrum of the RCs that are ^{13}C -enriched in BChl and BPhe, additional narrow signals from the labels are observed (Figure 4B).

Illumination of the site-directed ^{13}C -labeled and Q_A -reduced RCs with white light yields a photo-CIDNP response that is much stronger than the natural abundance ^{13}C response of the sample (Figure 4A). The recording time of the photo-CIDNP enhanced spectrum was only 20 min, very short compared to the 48 h recording time of a 1-D photo-CIDNP spectrum of unlabeled RCs (21). All enhanced signals are absorptive, corresponding with positive lines. This matches the earlier results from ^{13}C photo-CIDNP experiments in which the aromatic signals were also absorptive (39) and parallels ^{15}N photo-CIDNP experiments in which signals from P and I have the same sign (20). The aromatic MAS patterns comprise two sets of spinning sidebands upfield and downfield from the centerband response. 1-D photo-CIDNP MAS data sets were collected with different spinning frequencies and spinning sideband suppression (TOSS) was applied to identify the centerbands (21). For the data collected with $\omega_r/2\pi = 5$ kHz shown in Figure 4A, the overlap between spinning sidebands and centerbands is minimal. Several signals are observed in the aliphatic region of the spectrum collected in the “dark” that originate from the ^{13}C -8 and ^{13}C -17 in BChl or BPhe (Figure 4B). In the aromatic region, the responses from the ^{13}C -1, ^{13}C -3, ^{13}C -6, ^{13}C -11, ^{13}C -13, or ^{13}C -19 are detected between 125 and 175 ppm. For every photo-CIDNP signal, a corresponding line can be identified in the “dark” spectrum. To resolve the responses from the various labeled carbons, we calculated the second derivative of the 1-D photo-CIDNP spectrum of labeled RCs

and collected 2-D RFDR spectra. In Figure 5, the contour plots of a “dark” RFDR data set (left panel) and a photo-CIDNP RFDR data set (right panel) collected with long mixing times $\tau_m = 4.6$ ms and $\tau_m = 6$ ms, respectively, are shown.

The 1-D and 2-D RFDR data collected in the “dark” lead to the “dark” assignments in Table 1. They are confirmed with the set of 2-D ^{13}C - ^{13}C RFDR experiments collected in the “light”. The distances between the labeled carbons within a pyrrole ring, i.e., C-1/C-3, C-6/C-8, C-11/C-13, and C-17/C-19, are ~ 2.3 Å. For both the “dark” and “light” 2-D spectra, strong correlation signals are observed within a pair of enriched carbons in a pyrrole ring. In addition, cross-peaks between ^{13}C -1 and ^{13}C -19 are observed. In the 2-D “dark” spectrum, all six labeled cofactors, four BChl and two BPhe, can lead to such correlations, while in the 2-D “light” spectrum, only the cofactors that are enhanced by the photoinduced electron transfer are detected. The correlations in the photo-CIDNP RFDR NMR data set reveal a correlation network for the signals from two BChl molecules that are observed in the 1-D experiments and a network for the BPhe response. The two sets of BChl responses correspond with the strongest components in the 1-D spectrum and are assigned to the two BChl forming the special pair. They are denoted P1 and P2 since an unambiguous assignment of the NMR signals of the special pair to the A and B branch BChl was not yet achieved. The correlation networks observed for P1, P2, and BPhe are indicated separately in panels A, B, and C, respectively, of Figure 5, with the “dark” dataset in the left-hand panels and the “light” spectrum in the right-hand panels. The chemical shifts are listed in Table 1. An error of 0.3 ppm was estimated for the “light” spectra, and an error of 0.5 ppm was estimated for the “dark” spectra.

Special Pair BChl P1. For BChl and BPhe in solution, the aliphatic C-17 in acetone- d_6 resonate with 50.4 and 51.5 ppm shifts, respectively. The cluster of signals at 47–51 ppm in Figure 4A is thus assigned to the various C-17 in the RC preparation and can be used as a starting point for an assignment procedure. Strong correlations for C-17/C-19 are observed at 47.3/162.5 (P1), 49.7/159.7 (P2), and 52.5/169.9 (BPhe) ppm. For P1, the C-17/C-19 correlation in the “dark” spectrum is very strong compared to the other responses in the same area (Figure 5A, left panel). Probably the correlation response from C-17/C-19 of the P1 and the response of C-17/C-19 of the accessory BChls overlap. The assignment of the C-19 signal of the P1 is confirmed by the C-1/C-19 cross-peak at 148.2/162.5 ppm. A correlation between C-1 and C-3 is detected at 148.2/130.2 ppm.² The C-1 and C-3 in P1 are shifted upfield from their values in acetone- d_6 , 150.8 and 137.4 ppm, respectively. The distance between the C-1 label in ring I and the C-19 label in ring IV is also ~ 2.3 Å, and the C-1/C-19 cross-peaks are of similar intensity as those for the labeled carbons within a pyrrole ring. A connection between ring I and ring II could be obtained via C-3 and C-6 over a distance of ~ 3.8 Å. In the “light” RFDR spectrum with 6 ms mixing time, a weak correlation between C-3 and C-6 is detected at 130.2/166.8 ppm (Figure 5A, right panel), while the aromatic C-6 gives a correlation signal with the

² A cross-peak between C-1/C-3 is not observed, and therefore, the assignment of C-3 is not conclusive. The assignments of C-3 of BPhe and C-3 of monomeric BChl could be interchanged.

Table 1: ^{13}C —Chemical Shift Values of the ^{13}C Labeled Carbons in BChl and BPhe in the RC in Comparison with Chemical Shift Data from Solution NMR

carbon	BChl <i>a</i>				BPhe <i>a</i>	
	σ_{liq}^b	σ_{ss}^a			σ_{liq}^b	σ_{ss}^a
		P1	P2	B ^c		
1	150.8	148.2	143.4	148.5	139.7	138.3
3	137.4	130.2	127.6	133.2 ^d	134.8	134.7 ^d
6	168.4	166.8	164.6	167.0	170.9	171.1
8	55.6	53.0	55.4	50.6	55.4	54.6
11	149.4	150.3 ^e	154.2 ^e	149.4	139.3	138.9
13	130.3	131.0 ^e	131.3 ^e	130.2	129.3	126.4
17	50.4	47.3	49.7	48.7	51.5	52.5
19	167.1	162.5	159.7	162.7	169.8	169.9

^a The chemical shifts have been obtained from the photo-CIDNP spectra, and the estimated error in chemical shift is ± 0.3 ppm. ^b The liquid NMR data have been obtained in acetone-*d*₆. ^c The chemical shifts have been obtained from the “dark” spectra, and the estimated error in chemical shift is ± 0.5 ppm. ^d The chemical shift of C-3 of B and I could be interchanged. ^e The chemical shift combination of C-11/C-13 of P1 and P2 could be interchanged.

reveal considerable shifts for C-3 and C-19 of the P1 in the protein complex relative to monomeric BChl in solution. The aromatic C-3 and C-19 in P1 resonate with a shift of 130.2 and 162.5 ppm, respectively, which is 7.2 and 4.6 ppm upfield compared with the C-3 and C-19 responses of BChl in acetone-*d*₆.

Special Pair BChl P2. The response from the labels in rings I, II, and IV of the P2 can be assigned with a similar procedure as was followed for P1. In the “dark” RFDR spectrum, the P2 response is relatively weak, and only the correlations between aliphatic and aromatic nuclei (C-6/C-8 and C-17/C-19) are detected (Figure 5B, left panel). With illumination, the P2 response gives rise to a series of strong cross-peaks (Figure 5B, right panel). For instance, a strong correlation is observed for C-17/C-19 at 49.7/159.7 ppm. In addition, C-19 gives a cross-peak with C-1 at 159.7/143.4 ppm, and C-1 is also correlated with C-3 (143.4/127.6 ppm). The weaker correlation between C-3 and C-6 at 127.6/164.6 ppm provides a connection between signals from ring I and ring II, and finally C-6/C-8 gives a strong correlation at 164.6/55.4 ppm.

BPhe. An assignment for the BPhe is obtained from the data collected in the “dark” (Figure 5C, left panel). A correlation between C-17/C-19 is observed at 52.5/169.9 ppm, and the C-19/C-1 correlation is at 169.9/138.3 ppm. Since a correlation between C-1 and C-3 could not be detected, the C-3 was assigned based on a comparison with BPhe in acetone (134.8 ppm). In the 1-D “dark” spectra, two signals of approximately equal intensity are observed at 134.9 and 133.2 ppm, which are attributed to the C-3 responses of BPhe_A, BPhe_B, B_A, and B_B. Within the accuracy of the experiments, signals with the same shifts were observed in the 1-D “light” spectra (Figure 4A,B). The response at 134.9 ppm is assigned to C-3 of BPhe and the response at 133.2 ppm to C-3 of B. In the “dark” spectrum, the C-6/C-8 correlation is detected at 171.1/54.6 ppm. Finally, the correlation between C-11 and C-13 is observed at 138.9/126.4 ppm in both the “dark” and “light” spectra.

Monomeric BChl. Responses from the accessory BChls B_A and B_B are visible in the “dark” spectra and partially overlap with signals from P1. The C-17/C-19 cross-peak at

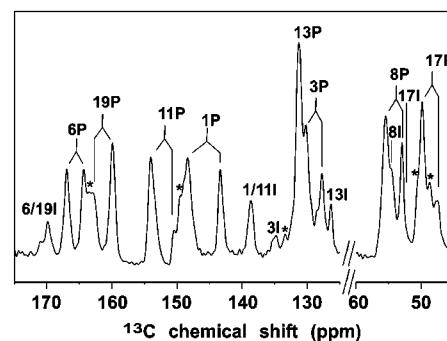


FIGURE 6: Expansions of the aromatic (175–125 ppm) and aliphatic (60–45 ppm) regions of the 1-D photo-CIDNP spectrum. Signals from the two BChls of the special pair (P) and the active BPhe (I) are assigned. The signals labeled with an asterisk (*) are attributed to a monomeric BChl cofactor.

47.3/162.5 is much stronger than the C-17/C-19 correlation of P2. This confirms that the C-17 and C-19 of P1 and the accessory BChls overlap. A weak correlation of C-1/C-19 is observed at 148.2/162.5 ppm. In the 1-D “dark” spectrum, a response at 133.2 ppm is tentatively assigned to C-3.² The C-6/C-8 cross-peak from B is observed at 167.0/50.6 ppm. The correlation between C-11/C-13 at 154.2/131.3 ppm appears to overlap with the correlation of C-11/C-13 of P1 or P2.

Photo-CIDNP MAS NMR. The spectra of the illuminated, Q_A reduced and selectively labeled RCs show strong nuclear spin polarization in the NMR responses of several ^{13}C -enriched carbons (Figure 6). A signal enhancement factor of $\sim 10^4$ is estimated, which is due to the combination of photo-CIDNP (~ 300 times) (16, 21, 39) and the enhancement due to the ^{13}C enrichment with $P_{\text{tot}} = 60\%$. Three cofactors (P1, P2 and BPhe) give rise to strong absorptive photo-CIDNP responses. Both the labels in the conjugated π -system (C-1, C-3, C-6, C-11, C-13, and C-19) and the enriched aliphatic ^{13}C -8 and ^{13}C -17 are strongly polarized. In previous studies with unlabeled RCs, no photo-CIDNP enhancement of the aliphatic carbons was detected (39, 40). It has been proposed that the polarization of C-8 and C-17 originates from polarized labeled aromatic carbon atoms, transferred by internuclear spin-diffusion processes (21).

Curve fitting of the 1-D photo-CIDNP spectrum with Lorentz curves reveals additional weaker signals in the regions 166–162, 151–148, 135–126, and 52–47 ppm. These signals are highlighted in Figure 6 by an asterisk (*). Several experiments with different spinning frequencies and using different samples confirm the authenticity of these signals. This fourth set matches the responses of C-6/C-19, C-1, C-11, C-3, and C-17 of a BChl.

DISCUSSION

Pronounced protein–pigment upfield shifts are observed for several carbons of P1, P2 and B, especially for C-3, C-8, and C-19, and indicate a stabilization of negative charge density compared to the chemical shifts of BChl in acetone-*d*₆ (Table 1). Solution ^{13}C NMR data showed that some ^{13}C chemical shifts of BChl are influenced by the coordination state of the magnesium ion (41). The magnesium ion is five-coordinated in acetone-*d*₆; therefore, this solvent was chosen for comparison with the results for BChl in the RC, where the magnesium is also five-coordinated by histidine residues.

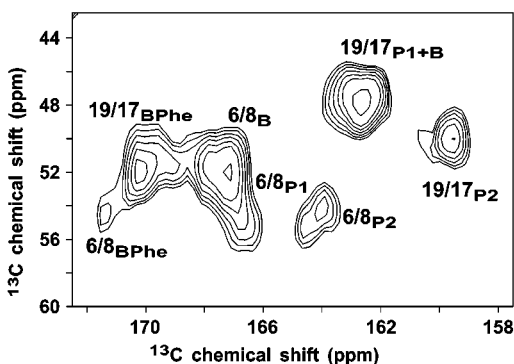


FIGURE 7: Aromatic–aliphatic expansion of the “dark” 2-D RFDR spectrum, revealing that three different BChl compounds (P1, P2, and B) and one BPhe are resolved.

The plot of the aromatic–aliphatic region (175–155/60–45 ppm) of the 2-D RFDR “dark” spectrum illustrates the sets of signals that are assigned to P1, P2, B, and BPhe (Figure 7). For the pairs in ring II, III, and IV, the chemical shifts in the B match the shifts observed for the P1. In contrast, ^{13}C responses from the labels in ring I of P1 are shifted, due to the ring current in P2 that results from the overlap of ring I of P1 and P2 within the special pair with an intermolecular distance of ~ 3.5 Å. The intensity ratio of $\sim 3:1$ in the 1-D “dark” spectra confirm that the shifts for the two B’s and P1 are similar, while the remaining P2 yields a shifted response. The photo-CIDNP MAS NMR spectra confirm that this shifted cofactor is the other BChl of the special pair. The responses from the P2 are shifted upfield by 2–5 ppm in ring I and IV compared to P1.

These NMR results are well in line with resonance Raman data that revealed for B and one BChl of P, compared to BChl in solution, a similar vibrational structure, with the other BChl of P being different (42).

Regarding the BPhe, the NMR assignments and intensities in the 1-D spectra suggest that both BPhe cofactors are similar in their electronic structure and that the chemical shifts correspond with the shifts observed for BPhe in solution (Table 1). This matches vibrational data and recent ^{13}C MAS NMR data collected from RCs of *Rb. sphaeroides* R26 reconstituted with $[U-^{13}\text{C}]$ -Phe *a* from plants, which also revealed only minor differences in chemical shifts between Phe in solution and Phe in the bacterial RC (42, 43).

Pronounced Asymmetry of P in the Ground State. Ground-state tuning of P is considered to be important to facilitate emission of an electron in the electronically excited state. It can be accomplished by local electrostatic interactions with the protein, e.g., via histidine ligation of the Mg^{2+} ion or hydrogen bonding to the ring keto functionality. When the hydrogen bond environment of P is changed by mutagenesis, the oxidation potential of P is also altered (44, 45). Analysis of the spin density distribution of the unpaired electron in the cation radical state of P in these mutant RCs by electron–nuclear–nuclear triple resonance also revealed that electrostatic interactions of P with nearby amino acids can influence the midpoint potential (46).

It is obvious from the NMR data that the electronic structure of the special pair is asymmetric in the ground state, since the chemical shifts for the positions C-1, C-3, C-6, C-11, and C-19 differ between P1 and P2. The differences $\Delta\sigma = \sigma_{\text{ss}} - \sigma_{\text{liq}}$ in upfield chemical shifts of the two BChls

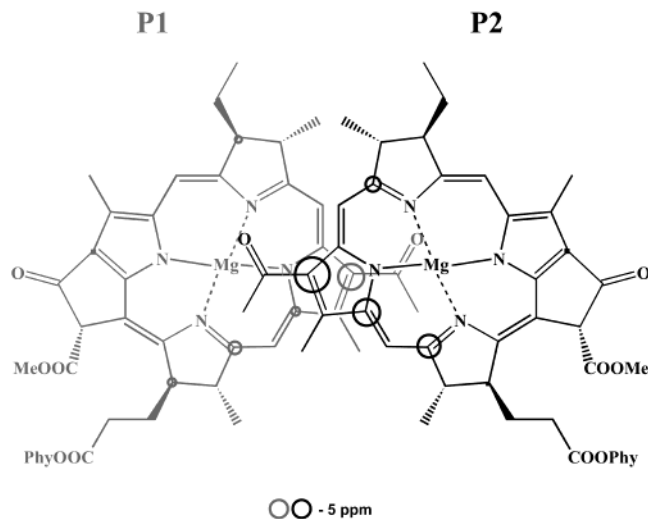


FIGURE 8: Visual representation of the upfield carbon shifts of the two BChls of P compared with data collected from monomeric BChl in acetone. The size of the circles measures the magnitude of the shifts.

of P compared to the values from solution NMR are visualized in Figure 8 by circles. From this figure, it transpires that for one BChl the electron density is shifted toward pyrrole ring I, II, and IV in the electronic ground state. The upfield shifts of the C-3 carbons are only partly explained by the ring current effect. The extensive delocalization of electrons in a porphyrin system can give rise to deshielding of ~ 2 – 3 ppm for nuclei located above one of the pyrrole rings at a distance of 3.5 Å (47). The upfield shifts of C-1, C-3, C-6, and C-19 of P2 are within a range of ~ 4 – 10 ppm and are therefore too large to be explained by ring current shifts only. Besides several upfield shifts, there was only one significant downfield shift $\Delta\sigma = 5.4$ ppm for the C-11 of either P1 or P2 (Table 1). For aromatic systems, a change in charge density of 1 electronic equivalent corresponds to a ^{13}C shielding of ~ 155 ppm (48, 49). The large upfield shifts of P2 indicate a significant stabilization of ~ -0.05 electronic equivalent negative charge per atom for both the C-3 and C-19 of the P2 relative to the monomeric solution, while the negative charge stabilization for P1 is less than for P2.

An important factor that could explain the observed electronic asymmetry between P1 and P2 and the differences compared to BChl in acetone is the hydrogen bonding environment. According to recent X-ray data, P–BChl_L is hydrogen bonded to His L168 via the 3-acetyl group (2, 4, 10), which is oriented out of the plane of the aromatic macrocycle. Both the presence of a hydrogen bond and the conformational twist can have an effect on the electronic structure and the corresponding chemical shifts. Since P2 is different from the other BChl cofactors and only the P–BChl_L is hydrogen bonded, we tentatively assign P2 to P–BChl_L. Our limited set of eight labels thus indicates a ground state with excess negative charge on the BChl_L relative to the BChl_M, which contrasts with the excited state difference $\text{BChl}_L^{\delta+}\text{BChl}_M^{\delta-}$ inferred from absorption and Stark spectroscopy (12).

Photo-CIDNP MAS NMR Observation Suggests Electronic Spin Density at the Accessory BChl. In the photo-CIDNP data, a fourth component is present, which gives rise to

absorptive signals with substantially less intensity than those for P1, P2, and BPhe. Since the same signals appear in the "dark" spectra, a transient form of a BChl cofactor of P that changes during the photoreaction cannot be the origin of the fourth component. It is also unlikely that the weak component is due to gross sample heterogeneity, since in that case multiple sets of P1, P2, and BPhe would be expected. Possibly B obtains some polarization during one of the stages of the photoreaction. Nuclear Overhauser transfer from an adjacent BChl that is directly polarized would contrast a recent photo-CIDNP observation of very weak polarization on ^{13}C -isotope-labeled tyrosine residues within the bacterial RC (40).

In the analysis of Figure 6, the signal intensities of the various ^{13}C responses from the polarized cofactors P1, P2, BPhe, and the minor BChl component, which is assigned to B, are extracted from the data by the Lorentz curve fitting. The average intensity ratio, integrated over the responses from every photo-CIDNP active cofactor is P1:P2:BPhe:B \approx 8:9:3:2.

The photo-CIDNP signal intensity is related to the electron spin density (19). For a single ^{13}C response, the intensity is affected by, e.g., spin diffusion processes or relaxation (18, 21). The CIDNP data suggest that illumination with white light generates spin density on B. This is in line with recent findings that charge separation can also occur from B^* (50).

The relative intensities of the aliphatic carbons C-8 and C-17 and the aromatic carbons C-11 and C-19 of P1 and P2 are \sim 1:2. This matches results from ^1H -ENDOR investigations of $\text{P}^{\bullet+}$ of several purple bacteria, which revealed a distribution of spin density over the two BChl molecules of the dimer with a ratio of approximately 1:2 in favor of P-BChl_L (11, 51, 52). This supports our assignment of P2 to P-BChl_L. Interestingly, for the aromatic carbons C-1, C-3, and C-6 the relative intensities are in our experiments different, \sim 1:1.

The integrated signal from BPhe is much less than the combined response of P1 and P2. On the other hand, the ^{15}N signals of BPhe are stronger than the signals from the two BChls of P (20). This could be due to a difference in the electron spin distribution for the two types of cofactors. In the HOMO of BChl, the electron spin is mainly localized on the carbons, while the electron spin distribution in the LUMO of BPhe is mainly localized on the nitrogens (53, 54).

Electronic Ground State of P is Largely Conserved during the Photoreaction and Recombination. An essential parameter in electron transfer is the reorganization energy, which reflects a rearrangement of the nuclear configuration associated with the charge-transfer process (7). Structural changes of the protein and or cofactors during the photoreaction can contribute to this reorganization energy. The chemical shifts of the responses in the spectra that were recorded in the "dark" were compared to the shifts recorded with illumination. Within the experimental uncertainty of 0.5 ppm, the shifts remain unchanged. Hence, according to our data, the rings of P and I are in virtually the same nuclear configuration, before and after illumination on the NMR shift scale. This corroborates previous CP MAS NMR results of [$4\text{-}^{13}\text{C}$]-tyrosine-enriched RCs from *Rb. sphaeroides* R26 (25, 55), which indicated that the protein complex in the vicinity of P is very rigid.

CONCLUSIONS

Site-directed multispin labeling, in combination with solid-state MAS NMR, has been used to investigate the electronic structure of a bacterial photosynthetic RC. CP/MAS and photo-CIDNP MAS NMR experiments have shown that the electronic structure of the special pair is asymmetric in the ground state. Comparison of ^{13}C NMR data of BChl in the RC and in acetone reveals stabilization of negative charge density on the ring carbons of the BChl of P. Photo-CIDNP MAS NMR data reveal electron spin density that is not only distributed over P and I, but also over B. The resemblance between the chemical shifts in the CP and photo-CIDNP MAS NMR spectra indicate that the electronic structure around the labeled atoms is not altered after illumination and recombination.

At this point, only the ^{13}C chemical shifts of eight of the 20 macrocycle carbons of the porphyrin cofactors have been determined. Future labeling experiments will enable the determination of the complete electronic structure of the macrocycles of the BChl and BPhe cofactors in the RC of *Rb. sphaeroides* WT.

ACKNOWLEDGMENT

The authors thank B. M. M. Joosten for the help in the purification of the RCs and B. Hofte and B. Karabatak for assistance with mass spectroscopy. The kind help of J. G. Hollander, C. Erkelens, and F. Lefeber during various stages of the NMR experiments is gratefully acknowledged.

REFERENCES

1. Michel, H., Weyer, K. A., Gruenberg, H., Dunger, I., Oesterhelt, D., and Lottspeich, F. (1986) *EMBO J.* 5, 1149–1158.
2. Chang, C.-H., Tiede, D., Tang, J., Smith, U., Norris, J., and Schiffer, M. (1986) *FEBS. Lett.* 205, 82–86.
3. Allen, J. P., Feyer, G., Yeates, T. O., Rees, D. C., Deisenhofer, J., Michel, H., and Huber, R. (1986) *Proc. Natl. Acad. Sci. U.S.A.* 83, 8589–8593.
4. Yeates, T. O., Komiya, H., Chirino, A., Rees, D. C., Allen, J. P., and Feher, G. (1988) *Proc. Natl. Acad. Sci. U.S.A.* 85, 7993–7997.
5. Zouni, A., Witt, H. T., Kern, J., Fromme, P., Krauss, N., Saenger, W., and Orth, P. (2001) *Nature* 409, 739–743.
6. Martin, J.-L., Breton, J., Hoff, A. J., Migus, A., and Antonetti, A. (1986) *Proc. Natl. Acad. Sci. U.S.A.* 38, 957–961.
7. Marcus, R. A., and Sutin, N. (1985) *Biochim. Biophys. Acta* 811, 265–322.
8. Lin, X., Murchison, H. A., Nagarajan, V., Parson, W. W., Allen, J. P., and Williams, J. C. (1994) *Proc. Natl. Acad. Sci. U.S.A.* 91, 10265–10269.
9. Ermler, U., Fritzsche, G., Buchanan, S. K., and Michel, H. (1994) *Structure* 2, 925–936.
10. Mattioli, T. A., Hoffmann, A., Robert, B., Schrader, B., and Lutz, M. (1991) *Biochemistry* 30, 4648–4654.
11. Rautter, J., Lendzian, F., Lubitz, W., Wang, S., and Allen, J. P. (1994) *Biochemistry* 33, 12077–12084.
12. Moore, L. J., Zhou, H. L., and Boxer, S. G. (1999) *Biochemistry* 38, 11949–11960.
13. Marassi, F. M., and Opella, S. J. (1998) *Curr. Opin. Struct. Biol.* 8, 640–648.
14. de Groot, H. J. M. (2000) *Curr. Opin. Struct. Biol.* 10, 593–600.
15. Soede-Huijbregts, C., Cappon, J. J., Boender, G.-J., Raap, J., Gast, P., Hoff, A. J., Lugtenburg, J., and de Groot, H. J. M. (1998) in *Photosynthesis: Mechanisms and Effect* (Garab, G., Ed.) pp 759–762, Kluwer Academic Publishers, Dordrecht, The Netherlands.
16. Zysmilich, M. G., and McDermott, A. E. (1994) *J. Am. Chem. Soc.* 116, 8362–8363.
17. Jeschke, G. (1998) *J. Am. Chem. Soc.* 120, 4425–4429.

18. McDermott, A. E., Zysmilich, M. G., and Polenova, T. (1998) *Solid State Nucl. Magn. Res.* 11, 21–47.
19. Polenova, T., and McDermott, A. E. (1999) *J. Phys. Chem. B* 103, 535–548.
20. Zysmilich, M. G., and McDermott, A. E. (1996) *J. Am. Chem. Soc.* 118, 5867–5873.
21. Matysik, J., Schulten, E., Alia, Gast, P., Raap, J., Lugtenburg, J., Hoff, A. J., and de Groot, H. J. M. (2001) *Biol. Chem.* 382, 1271–1276.
22. Jordan, P. M. (1991) in *Biosynthesis of Tetrapyrroles* (Jordan, P. M., Ed.) pp 1–66, Elsevier, Amsterdam.
23. Burton, G., Baxter, R. L., Gunn, J. M., Sidebottom, P. J., Fagerness, P. E., Shishido, K., Lee, J. Y., and Scott, A. I. (1980) *Can. J. Chem.* 58, 1839–1846.
24. Akthar, M., Ajaz, A. A., and Corina, D. L. (1984) *Biochem. J.* 224, 187–194.
25. Shochat, S., Arlt, T., Francke, C., Gast, P., van Noort, P. I., Otte, S. C. M., Schelvis, H. P. M., Schmidt, S., Vijgenboom, E., Vrieze, J., Zinth, W., and Hoff, A. J. (1994) *Photosynthesis Res.* 40, 55–66.
26. Beale, S. I., and Weinstein, J. D. (1991) in *Biosynthesis of Tetrapyrroles* (Jordan, P. M., Ed.) pp 155–235, Elsevier, Amsterdam.
27. Clayton, R. K. (1966) *Photochem. Photobiol.* 5, 669–677.
28. Biemann, K. (1962) in *Mass Spectrometry: Organic Chemical Applications*, pp204–250, McGraw-Hill book company, New York.
29. Boender, G.-J., and Vega, S. (1998) *J. Magn. Res.* 133, 281–285.
30. Gullion, T., and Vega, S. (1992) *Chem. Phys. Lett.* 194, 423–428.
31. Bennett, A. E., Ok, J. H., Griffin, R. G., and Vega, S. (1992) *J. Chem. Phys.* 96, 8624–8627.
32. Bruker (1999) *XWIN-NMR Software Manual; Part 1 General Features and Data Processing*, Bruker Analytik GmbH, Karlsruhe, Germany.
33. Matysik, J., Alia, Hollander, J. G., Egorova-Zachernyuk, T. A., Gast, P., and de Groot, H. J. M. (2000) *Indian J. Biochem. Biophys.* 37, 418–423.
34. Bennett, A. E., Rienstra, C. M., Auger, M., Lakshmi, K. V., and Griffin, R. G. (1995) *J. Chem. Phys.* 103, 6951–6958.
35. Dixon, W. T. (1982) *J. Chem. Phys.* 77, 1800–1809.
36. Porra, R. J. (1997) *Photochem. Photobiol.* 65, 492–516.
37. Spikes, J. D., and Bommer, J. C. (1991) in *Chlorophylls* (Scheer, H., Ed.) pp 1181–1204, CRC Press, Boca Raton, FL.
38. Schrott, E. L. (1985) *Pure Appl. Chem.* 57, 729–734.
39. Zysmilich, M. G., and McDermott, A. E. (1996) *Proc. Natl. Acad. Sci. U.S.A.* 93, 6857–6860.
40. Matysik, J., Alia, Gast, P., van Gorkom, H. J., Hoff, A. J., and de Groot, H. J. M. (2000) *Proc. Natl. Acad. Sci. U.S.A.* 97, 9865–9870.
41. Abraham, R. J., and Rowan, A. E. (1991) in *Chlorophylls* (Scheer, H., Ed.) pp 797–834, CRC Press, Boca Raton, FL.
42. Palaniappan, V., Martin, P. C., Chynwat, V., Frank, H. A., and Bocian, D. F. (1993) *J. Am. Chem. Soc.* 115, 12035–12049.
43. Egorova-Zachernyuk, T. A., van Rossum, B., Boender, G.-J., Franken, E., Ashurst, J., Raap, J., Gast, P., Hoff, A. J., Oschkinat, H., and de Groot, H. J. M. (1997) *Biochemistry* 36, 7513–7519.
44. Mattioli, T. A., Lin, X., Allen, J. P., and Williams, J. C. (1995) *Biochemistry* 34, 6142–6152.
45. Ivancich, A., Artz, K., Williams, J. C., Allen, J. P., and Mattioli, T. A. (1998) *Biochemistry* 37, 11812–11820.
46. Artz, K., Williams, J. C., Allen, J. P., Lenzian, F., Rautter, J., and Lubitz, W. (1997) *Proc. Natl. Acad. Sci. U.S.A.* 94, 13582–13587.
47. Giessner-Prettre, C., and Pullman, B. (1971) *J. Theor. Biol.* 31, 287–294.
48. Spiesecke, H., and Schneider, W. G. (1961) *Tetrahedron Lett.* 14, 468–472.
49. Tokuhito, T., and Fraenkel, G. (1969) *J. Am. Chem. Soc.* 91, 5005–5013.
50. Van Brederode, M. E., Jones, M. R., Van Mourik, F., Van Stokkum, I. H. M., and Van Grondelle, R. (1997) *Biochemistry* 36, 6855–6861.
51. Lenzian, F., Lubitz, W., Scheer, H., Hoff, A. J., Plato, M., Trankle, E., and Möbius, K. (1988) *Chem. Phys. Lett.* 148, 377–385.
52. Lenzian, F., Huber, M., Isaacson, R. A., Endeward, B., Plato, M., Bonigk, B., Möbius, K., Lubitz, W., and Feher, G. (1993) *Biochim. Biophys. Acta* 1183, 139–160.
53. Plato, M., Möbius, K., and Lubitz, W. (1991) in *Chlorophylls* (Scheer, H., Ed.) pp 1015–1046, CRC Press, Boca Raton, FL.
54. Plato, M., Lenzian, F., Lubitz, W., and Möbius, K. (1992) in *The Photosynthetic Bacterial Reaction Center II: Structure, Spectroscopy and Dynamics* (Breton, J., and Vermeglio, A., Eds.) pp 109–118, Plenum Press, New York.
55. Fischer, M. R., de Groot, H. J. M., Raap, J., Winkel, C., Hoff, A. J., and Lugtenburg, J. (1992) *Biochemistry* 31, 11038–11049.

BI025608U